

# Journal of Materials Chemistry A

Accepted Manuscript



This is an *Accepted Manuscript*, which has been through the Royal Society of Chemistry peer review process and has been accepted for publication.

*Accepted Manuscripts* are published online shortly after acceptance, before technical editing, formatting and proof reading. Using this free service, authors can make their results available to the community, in citable form, before we publish the edited article. We will replace this *Accepted Manuscript* with the edited and formatted *Advance Article* as soon as it is available.

You can find more information about *Accepted Manuscripts* in the [Information for Authors](#).

Please note that technical editing may introduce minor changes to the text and/or graphics, which may alter content. The journal's standard [Terms & Conditions](#) and the [Ethical guidelines](#) still apply. In no event shall the Royal Society of Chemistry be held responsible for any errors or omissions in this *Accepted Manuscript* or any consequences arising from the use of any information it contains.

# Highly-sensitive SnO<sub>2</sub> Nanofiber Chemiresistors with Low Optimal Operating Temperature: Synergistic Effect of Cu<sup>2+</sup>/Au Co-doping†

Cite this: DOI: 10.1039/x0xx00000x

Zhenyu Li,<sup>a,b</sup> Xungai Wang<sup>a</sup> and Tong Lin<sup>a\*</sup>

Received 00th January 2012,  
Accepted 00th January 2012

DOI: 10.1039/x0xx00000x

www.rsc.org/

Metal oxide chemiresistors (MOCs) with a low optimal operating temperature, high sensitivity and fast response/recovery are highly promising for various applications, but remain challenging to realize. Herein, we demonstrate that SnO<sub>2</sub> nanofibers after being co-doped with Cu<sup>2+</sup> and Au show considerably enhanced sensing performances at an unexpectedly-decreased operating temperature. A synergistic effect occurs when the two dopants are introduced together. Co-doping may form a novel strategy to development of ultrasensitive MOCs working at a low optimal temperature.

## Introduction

Metal oxide chemiresistors (MOCs), which can monitor gas or vapor based on resistance change, often have high sensitivity, low cost and compatibility with microelectronic processing. They show promising applications in environment, health, security and automotive sectors.<sup>1-5</sup> MOCs from a nanostructured metal oxide are of particular interest because the large surface-to-volume ratio allows the exposure of as much as possible sensing sites on the surface, offering cutting-edge sensing ability (e.g. rapid adsorption/desorption).<sup>6-17</sup> Most of the MOCs, however, have to work at a temperature typically above 200 °C, which consumes large energy. The oxide grains during working at a high temperature may coalesce, undermining the sensing performance. High working temperature also confines the use of MOCs for explosive detection.<sup>11</sup>

Efforts to lower the operating temperature of MOCs have been reported by several groups. Approaches include improving the conductivity of metal oxides, increasing the amount of ionosorbed oxygen species on metal oxide surface, or enhancing interactions between target molecules and ionosorbed oxygen species of the metal oxide. For examples, carbon nanotubes<sup>18-21</sup> or graphene<sup>22-26</sup> were added to improve the conductivity of metal oxides at a low temperature; and nonstoichiometric metal oxides were employed to increase the ionosorbed oxygen species on oxide surface.<sup>27-30</sup> UV-light irradiation was also reported to reduce MOC operating temperature because UV-light irradiation could increase not only the conductivity of metal oxides but also the ionosorbed oxygen species on the metal oxide.<sup>31-35</sup> Despite the success in lowering the operating temperature, the MOCs reported often had low response and recovery speeds (e.g. larger than 1 min), which were attributed to weak interactions between target molecules and metal oxide, leading to inevitable delay in monitoring of target states.

Doping metal oxide with a noble metal, such as Au, is an effective route to reduce the activation energy ( $E_a$ ) of reaction between target molecules and ionosorbed oxygen species,<sup>36</sup> which has been widely used to enhance the sensing performance of MOCs.<sup>37-40</sup> Nevertheless, Au doping normally shows finite change in MOC operating temperature. In contrast, doping with an extrinsic metal ion was reported to considerably increase ionosorbed oxygen species on metal oxide surface, which is derived from the increased oxygen vacancies in the host crystals because of the mismatch between the two metal ions.<sup>41-43</sup> However, whether co-doping with both an extrinsic metal ion and noble metal can increase the sensitivity but decrease the optimal operating temperature of a MOC has not been reported in research literature.

Herein, we demonstrate a novel strategy to increase MOC sensitivity and meanwhile lower the optimal operating temperature by co-doping metal oxide with metal ions and noble metal. Electrospinning was employed to prepare SnO<sub>2</sub> nanofibers containing both Cu<sup>2+</sup> and Au. The Cu<sup>2+</sup>/Au co-doped SnO<sub>2</sub> nanofiber MOCs had an optimal operating temperature (160 °C) to detect acetylene (C<sub>2</sub>H<sub>2</sub>), almost 100 °C lower than those made of pristine SnO<sub>2</sub> nanofibers or SnO<sub>2</sub> nanofibers just doped by Cu<sup>2+</sup> or Au. The co-doping caused a synergistic effect which considerably enhanced the sensitivity. Acetylene is selected because it is often generated in oil-filled power equipment, such as large power transformers. The detection of C<sub>2</sub>H<sub>2</sub> gas is important for on-site monitoring the working state and diagnosing the fault of oil-filled power equipment.

## Experimental

### Materials

SnCl<sub>2</sub>·2H<sub>2</sub>O was acquired from Tianjin Chemical Co. and Cu(NO<sub>3</sub>)<sub>2</sub>·3H<sub>2</sub>O from Beijing Chemical Co. Ethanol, N, N'-

dimethylformamide (DMF), poly(vinyl pyrrolidone) (PVP,  $M_w = 1,300,000$ ) and gold(III) chloride trihydrate were obtained from Aldrich. All materials were used as received. The solution for electrospinning was prepared by dissolving  $\text{SnCl}_2 \cdot 2\text{H}_2\text{O}$  (0.4 g) in a solvent mixture of DMF (4.4 g) and ethanol (4.4 g) under vigorous stirring. PVP (0.8 g),  $\text{Cu}(\text{NO}_3)_2 \cdot 3\text{H}_2\text{O}$  and gold(III) chloride trihydrate were then added into the solution, and a homogeneous solution was formed by further stirring vigorously for 30 min. The Au/Sn atomic ratio in the solution was kept at 5:100, and Cu/Sn atomic ratio was controlled at 1:100, 2:100, and 3:100. For comparison, solutions without containing elements Cu and Au were also prepared using the same procedure.

### Preparation of nanofibers

Precursor nanofibers were prepared using a purposely made electrospinning setup consisting of a high voltage power supply, a glass syringe (inner diameter, 1 mm) and a metal plate collector. The solution prepared was placed into the syringe. A high DC voltage (15 kV) was then applied between the syringe needle tip and the collector (distance 20 cm). Fibers were electrospun from the syringe needle and deposited onto the collector. After electrospinning, the precursor fibers were peeled off the collector and then calcined at 600 °C in air for 5 hours.

### Fabrication and MOC sensor

The nanofibers prepared were mixed with deionized water at a fiber/water ratio of 100:15 (wt/wt), and the mixture was ground into a paste, which was spin-coated onto a ceramic tube on which a pair of gold electrodes was pre-printed. A Pt heating wire was inserted into the tube to form a side-heated gas sensor. The sensor device was dried for 2 days at room temperature. Prior to gas sensing measurement, all the MOC device (nanofibers with ceramic tube) were aged at 350 °C for 12 h. During the measurement, all the devices were stabilized at each testing temperature for at least 6 h.

### Characterizations of sensor property

Sensing properties were measured using a static flow system, which composed a heater, a gas distributor and a data acquisition system. Resistance change was recorded during exposing the sensor device to  $\text{C}_2\text{H}_2$ -containing air, using the CGS-8 intelligent test system (Beijing Elite Tech Co. Ltd., China). When the response reached a constant value, the device was then recovered by exposing to pure air. The gas sensor response ( $R_a/R_g$ ) was defined as the device resistance ratio in air ( $R_a$ ) and in testing gas ( $R_g$ ).<sup>44</sup> The test was performed in a temperature range of 120 °C ~ 300 °C. The response time was defined as the time taken by the sensor device to achieve 90% change of the resistance during exposure in the test gas, while the recovery time was defined as the time required for recovery of 90% resistance in pure air.<sup>45</sup>

### Other characterizations

The morphologies and structures of the samples were investigated by transmission electron microscopy (TEM) on a

JEOL-2100 with an acceleration voltage of 200 kV and the scanning electron microscope (SEM Supra 55VP). Crystal structures were measured by X-ray diffraction (XRD, Scintag XDS 2000 diffractometer with a Cu K $\alpha$  radiation). X-ray photoelectron spectra (XPS) was measured on an ESCLAB MKII using Al as the exciting source. All peaks in the XPS survey spectrum were calibrated based on the binding energy of C1s (284.6 eV). Surface area was measured using the BET nitrogen adsorption method on Micromeritics ASAP2000. The pore size distribution was derived by the Barret–Joyner–Halenda method. To measure the electrical resistance of  $\text{SnO}_2$  nanofiber sample, a pair of gold electrodes (thickness 100 nm) with 60  $\mu\text{m}$  channel spacing was evaporated onto a  $\text{SiO}_2$  wafer. Nanofiber sample (1 mg) was dispersed in 200  $\mu\text{L}$  distilled water. After ultrasonication for 2 minutes, 10  $\mu\text{L}$  nanofiber dispersion was dropped into the channel spacing, and the electrode was finally dried.

## Results and Discussion

### Morphology and crystalline structure

Cu/Au co-doped  $\text{SnO}_2$  nanofibers (CASNFs) were prepared by electrospinning of a PVP solution containing  $\text{SnCl}_2$ ,  $\text{Cu}(\text{NO}_3)_2$  and gold(III) chloride to get precursor nanofibers and by subsequent calcination of the precursor nanofibers at 600 °C in air to remove the polymer component and form  $\text{SnO}_2$  crystal phase. Fig. 1a shows the typical SEM image of the CASNFs (molar ratio of Cu/Au/Sn is 1:5:100, also referred to as 1Cu/5Au/ $\text{SnO}_2$ ), indicating a porous structure with lots micro-pores between the adjacent CASNFs. Nano-pores among the agglomerated gains throughout the CASNFs can be clearly seen under the image of higher magnification (inset of Fig. 1a). For comparison, the SEM images of pristine  $\text{SnO}_2$  nanofibers without Au and Cu, prepared by the same method, is presented in Fig. 1b. The pristine  $\text{SnO}_2$  nanofibers showed a similar morphology to CASNFs. Variation of Cu/Sn ratio in CASNFs was found to have little effect on the fiber morphology (see ESI†).

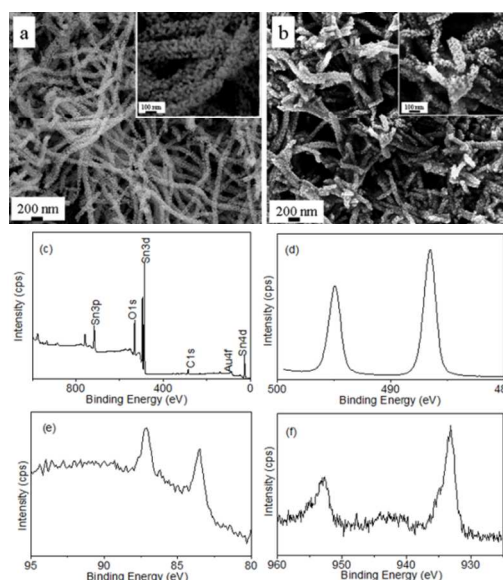


Fig. 1 a) & b) SEM images of a) CASNFs and b) pristine SnO<sub>2</sub> nanofibers, c) XPS survey spectrum, d) ~ f) XPS high resolution d) Sn3d, e) Au4f, and f) Cu2p spectra. (CASNFs for b ~ f based on 1Cu/5Au/SnO<sub>2</sub>).

The formation of porous nanofibers was derived from removal of the PVP component from the fibers and crystallization of metal oxides, which was similar to other metal oxide nanofibers prepared by an electrospinning route.<sup>46</sup> The porous fiber structure is preferable to the absorption of target molecules for gas detection.<sup>36</sup>

X-ray photoelectron spectroscopy (XPS) was used to examine the surface chemical component of CASNFs. Fig. 1c shows the survey spectrum of CASNFs (1Cu/5Au/SnO<sub>2</sub>), indicating the existence of elements Sn, C, Au, Cu and O on nanofiber surface. The high resolution XPS Sn3d spectrum in Fig. 1d shows two symmetric peaks with binding energy at 494.9 eV and 486.4 eV, which are assigned to Sn3d<sub>3/2</sub> and Sn3d<sub>5/2</sub>. The well separated spin-orbit components between the two peaks ( $\Delta_{metal} = 8.5$  eV) indicated that the element Sn was in Sn<sup>4+</sup> state.<sup>47</sup> The high resolution Au4f spectrum showed two peaks at 83.4 eV and 87.8 eV, corresponding to Au4f<sub>7/2</sub> and Au4f<sub>5/2</sub>, respectively (Fig. 1e). Since no peaks were located at around 85.5 eV and 86.3 eV, which are the characteristic binding energies of oxidized Au, Au in CASNFs was in metallic state. In contrast to bulk metallic Au (84.1 eV), the Au in nanofibers had a negative shift (-0.7 eV) in binding energy. This indicates strong interaction between Au and SnO<sub>2</sub> (e.g. electron transfer from SnO<sub>2</sub> to Au<sup>15</sup>). For element Cu, the 2p<sub>3/2</sub> and 2p<sub>1/2</sub> peaks were detected at 932.1 eV and 952.0 eV (Fig. 1f). The satellite peak at higher binding energy confirms the chemical state of Cu ions is Cu<sup>2+</sup> in the final products.<sup>48</sup>

Fig. 2 shows the XRD patterns of SnO<sub>2</sub> nanofibers. SnO<sub>2</sub> in CASNFs had the characteristics of tetragonal rutile SnO<sub>2</sub> crystal phase (JCPDS 41-1445), while Au was in face centered cubic crystal phase (JCPDS No. 65-2870). Since no peaks associated with copper oxide phase was detected, long order CuO lattice was not formed in the CASNFs.

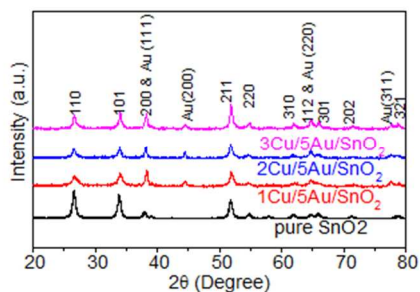


Fig. 2 XRD patterns of CASNFs and pure SnO<sub>2</sub> nanofibers.

Au and Cu<sup>2+</sup> in SnO<sub>2</sub> nanofibers were examined by a TEM EDS mapping technique (see the images in ESI†). It was interesting to note that Au existed in the form of particles scattering in the nanofibers, while element Cu distributed throughout the entire nanofibers. Despite the dispersion state, “doping” here was still used to specify the effect of Cu<sup>2+</sup> ion and Au nanoparticles on SnO<sub>2</sub> nanofibers.

High-resolution XRD was employed to examine the effect of Cu<sup>2+</sup> on SnO<sub>2</sub> on Au crystal phase. The SnO<sub>2</sub> (101) peak was found to slightly shift to a lower angle when increasing the Cu<sup>2+</sup> doping level from 1 at% to 2 at% (see ESI†). Such a shift was attributed to a substitution mechanism upon incorporation of Cu<sup>2+</sup> ions into SnO<sub>2</sub> lattice network.<sup>49</sup> When the Cu<sup>2+</sup>-doping level was further increased to 3 at%, the peak recovered a little, indicating saturation of the Cu<sup>2+</sup> substitution in SnO<sub>2</sub> crystal.

By comparing the XRD patterns of 5Au/SnO<sub>2</sub> and 1Cu/5Au/SnO<sub>2</sub>, we noted that the presence of Cu<sup>2+</sup> ions in the Au-doped SnO<sub>2</sub> nanofibers led to increase of peak at  $2\theta=38^\circ$ , which corresponded to Au(111) crystal phase. The peak was higher than that of SnO<sub>2</sub>(110) and SnO<sub>2</sub>(101). For the SnO<sub>2</sub> nanofibers just doped with Au (*i.e.* 5Au/SnO<sub>2</sub>), however, the Au(111) peak was lower than that of the SnO<sub>2</sub>(110) and SnO<sub>2</sub>(101) (see ESI†). In addition, Au-doping did not affect the peaks of SnO<sub>2</sub> (200). These results suggest that Cu<sup>2+</sup>-doping facilitates the growth of Au(111) crystal phase, leading to increase in the catalytic ability.

### Sensing properties

Sensing property against C<sub>2</sub>H<sub>2</sub> was studied. Fig. 3a shows the gas sensor response ( $R_a/R_g$ ) of the MOC devices in 100 ppm C<sub>2</sub>H<sub>2</sub> at different operating temperatures. For the pristine SnO<sub>2</sub>, the response value increased with increasing the operating temperature until 260 °C. Further increasing the temperature led to decrease in the response value.<sup>36</sup> The response and recovery curve of the device in 100 ppm C<sub>2</sub>H<sub>2</sub> at 260 °C is shown in Fig. 3b. The response time and recovery time were both ~7s. Therefore, the optimal operating temperature of the pristine SnO<sub>2</sub> nanofiber MOC was 260 °C.

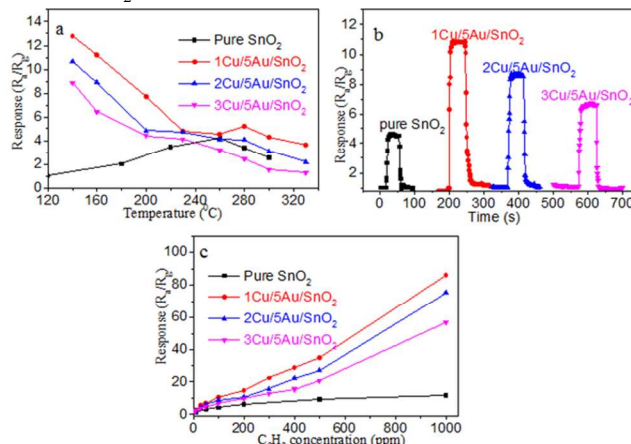


Fig. 3 a) Sensor response of MOC devices as a function of operating temperature (C<sub>2</sub>H<sub>2</sub> concentration, 100 ppm), b) response/recovery curves of MOC devices against 100 ppm C<sub>2</sub>H<sub>2</sub>, c) effect of C<sub>2</sub>H<sub>2</sub> concentration on sensor response. (in b and c, the working temperature for the pristine SnO<sub>2</sub> nanofiber and CASNFs was 260 °C and 160 °C, respectively).

For CASNF-based MOC devices, the response value decayed monotonically when the operating temperature increased from 140 °C to 320 °C. Here, 140 °C was selected as the lower limit of operating temperature for the reason that the device resistance became too large to be measured by the test

system when temperature was below this point. Among the CASNF devices, the one from 1Cu/5Au/SnO<sub>2</sub> had the highest response value. We also found that at 140 °C, CASNF MOCs exhibited long response/recovery behaviors, which could not be used to effectively monitor target molecules. When the working temperature reached 160 °C, the devices showed good response/recovery behavior. The respond and recovery curves of the CASNF devices in 100 ppm C<sub>2</sub>H<sub>2</sub> at 160 °C are shown in Fig. 3b. The response/recovery behaviors for CASNF devices were 5s/13s, 7s/6s, and 7s/6s for 1Cu/5Au/SnO<sub>2</sub>, 2Cu/5Au/SnO<sub>2</sub>, and 3Cu/5Au/SnO<sub>2</sub>, respectively. Therefore, 160 °C was identified to be the optimal operating temperature of the CASNFs. The effect of C<sub>2</sub>H<sub>2</sub> concentration on the response of MOCs is shown in Fig. 3c. At the optimal operating temperature, CASNF devices had higher response than pristine SnO<sub>2</sub> nanofiber device, although the former worked at a temperature 100 °C lower than the later.

We also quantitatively compared our results on sensing performances with those reported by researchers on MOCs for monitoring C<sub>2</sub>H<sub>2</sub> (see ESI†). It is clearly indicated that our CASNF MOCs exhibit better sensing performance than the previous reports.

To explore the role of Cu<sup>2+</sup>/Au co-doping in the enhancement of sensing performances, SnO<sub>2</sub> nanofibers containing just one dopant were prepared using the same method, and the fiber morphology, crystalline structure, and sensing performance were examined. SnO<sub>2</sub> nanofibers doped by Cu<sup>2+</sup> or Au showed a similar fiber morphology to CASNFs (see ESI†). The single dopant had little effect on fiber diameter. The XRD curves also confirmed that the dopants did not change the tetragonal rutile crystal characteristic of SnO<sub>2</sub> (JCPDS 41-1445) (see ESI†).

Fig. 4a shows the gas response of MOC devices made of SnO<sub>2</sub> nanofibers doped by Cu<sup>2+</sup> or Au. In 100 ppm C<sub>2</sub>H<sub>2</sub>, the Cu<sup>2+</sup> doped SnO<sub>2</sub> showed a similar response trend to the pristine SnO<sub>2</sub> nanofiber device. Cu<sup>2+</sup>-doping did not change the optimal operating temperature, but increased the response value and response/recovery behaviors (Fig. 4b).

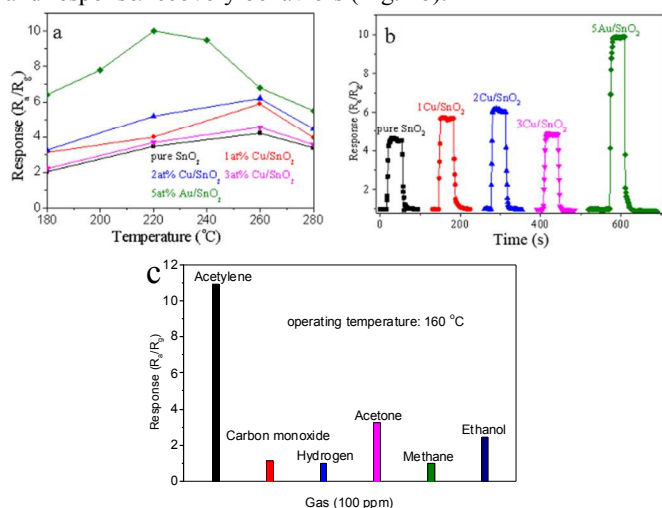


Fig. 4 a) MOC sensitivity of SnO<sub>2</sub> nanofibers doped by Cu<sup>2+</sup> or Au (in 100 ppm C<sub>2</sub>H<sub>2</sub>), b) response/recovery curves of the MOC devices against 100 ppm C<sub>2</sub>H<sub>2</sub> (the operating temperature was 260 °C for the Cu<sup>2+</sup>-doped SnO<sub>2</sub>, and 220 °C for the Au-doped SnO<sub>2</sub>), c) cross-response of MOC device (1Cu/5Au/SnO<sub>2</sub>).

For the Au-doped SnO<sub>2</sub> nanofibers, the MOC device had an optimal operating temperature of 220 °C, which was slightly lower than that of pristine SnO<sub>2</sub> nanofiber (260 °C), but higher than that of CASNF (160 °C). The response and recovery time of Au-doped device are 6s and 7s (Fig. 4b). The slightly decreased optimal operating temperature was explained by the spill-over and electronic (chemistry) sensitization of Au.<sup>50-52</sup>

The above sensing results clearly indicate that the co-doped SnO<sub>2</sub> nanofibers have much higher MOC response value than those just doped by single Cu<sup>2+</sup> or single Au. A synergistic effect on the gas response occurs when SnO<sub>2</sub> nanofibers are co-doped by Cu<sup>2+</sup> and Au.

We also tested the cross-response of our MOC device (1Cu/5Au/SnO<sub>2</sub>) to different gases, including carbon monoxide, hydrogen, acetone, methane and ethanol. As shown in Fig. 4c, the MOC device has a good sensing selectivity to acetylene.

To find out the source of the synergetic effect, we also measured the effect of Cu<sup>2+</sup> and Au on the electrical resistance, surface area and pore size of SnO<sub>2</sub> nanofibers. For pure SnO<sub>2</sub> nanofibers, the resistance measured by a two-probe method was 70 kΩ. Doping SnO<sub>2</sub> with Au or Cu considerably increased the resistance, respectively to 4×10<sup>5</sup> kΩ (Au 5 at%) and 2×10<sup>5</sup> kΩ (Cu 2 at%). Co-doping further increased the resistance. The resistance of Cu<sup>2+</sup>/Au co-doped SnO<sub>2</sub> nanofibers (1Cu/5Au/SnO<sub>2</sub>) was too large to be measured by our test system.

The BET surface area of all nanofiber samples is listed in Table 1 (see the detail result in ESI†). Cu<sup>2+</sup>-doping increased the surface area, while Au-doping led to a reverse trend. Co-doped SnO<sub>2</sub> nanofibers showed slightly lower surface area than the pure SnO<sub>2</sub> nanofibers.

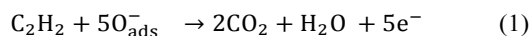
Table 1 BET surface area and pore size

Samples	Surface area (m <sup>2</sup> /g)	Pore size 1 (nm)	Pore size 2 (nm)
Pure SnO <sub>2</sub>	33.3	1.7	21.8
5Au/SnO <sub>2</sub>	30.5	1.5	25.9
2Cu/SnO <sub>2</sub>	64.8	2.1	20.4
1Cu/5Au/SnO <sub>2</sub>	32.0	1.6	20.7

The pores in the nanofiber samples showed a bimodal and wide size distribution (see ESI†). Here, the pore size values centered in the bimodal distribution are also listed in Table 1. Doping with Cu<sup>2+</sup> increased the size of smaller pores, but decreased the size of the larger pores. Au-doping showed a reverse change. When SnO<sub>2</sub> was co-doped with Au and Cu<sup>2+</sup>, both the large and the small pores were slightly reduced when compared with those in the pure SnO<sub>2</sub> nanofiber sample.

## Discussion

With using n-type semiconducting metal oxides as sensor medium, oxygen vacancies play a critical role in determining the sensing performance. To approach the stoichiometry of metal oxide, oxygen molecules are adsorbed on the surface. The oxygen species act as an electron acceptor to withdraw electrons from the conduction band of the metal oxides. Ionsorbed oxygen species are thus formed, resulting in an electron-depleted surface region (also called “space-charge layer”) and increase in electrical resistance. The ionsorbed oxygen species are reverted when exposed to reducing gas. In this way, the electrons trapped by the oxygen species feed back to the metal oxides, leading to decrease in the resistance. In our case, the reaction between C<sub>2</sub>H<sub>2</sub> and the ionsorbed oxygen species on SnO<sub>2</sub> is shown in equation (1).



The reaction coefficient ( $\alpha$ ) is governed by several factors and can be expressed as:<sup>36</sup>

$$\alpha = \alpha_0 \exp\left(-\frac{E_a}{RT}\right) \quad (2)$$

Where  $E_a$  is the activation energy of the reaction,  $\alpha_0$  is pre-exponential constant,  $T$  is reaction temperature and  $R$  is gas constant.

Introducing Au nanoparticles into SnO<sub>2</sub> nanofibers could lead to three scenarios: 1) reduction of the  $E_a$  owing to the catalytic effect of Au, which improves the reaction efficiency at a low temperature; 2) increasing the amount of ionsorbed oxygen species on SnO<sub>2</sub>,<sup>52</sup> thus strengthening the interactions between C<sub>2</sub>H<sub>2</sub> and the ionsorbed oxygen species and hence increasing the sensitivity; 3) increasing the height of space-charge layer, which also leads to enhanced sensitivity. The last scenario comes from the band structure. Since the working function of Au is typically lower than the Fermi level of SnO<sub>2</sub>, a Schottky barrier forms at Au-SnO<sub>2</sub> interface, electrons transfer from SnO<sub>2</sub> to Au.<sup>53</sup>

When SnO<sub>2</sub> is doped with Cu<sup>2+</sup>, the grain size of SnO<sub>2</sub> decreases because of the mismatched atomic radius between Cu<sup>2+</sup> (74 pm) and Sn<sup>4+</sup> (69 pm). The effect of Cu/Sn atomic ratio on the grain size of SnO<sub>2</sub> in the nanofibers is shown in ESI†, which is similar to previous report.<sup>54</sup> The reduction in SnO<sub>2</sub> grain size allows more active sites on the surface, which gives higher gas sensitivity.

The synergistic effect of Cu<sup>2+</sup>/Au co-doping was proposed. Cu<sup>2+</sup> doping increases the active sites on SnO<sub>2</sub> surface owing to the reduced SnO<sub>2</sub> grain size. Au nanoparticles in SnO<sub>2</sub> nanofibers also enhance the sensitivity. Since the presence of Cu<sup>2+</sup> in the Au-doped SnO<sub>2</sub> nanofiber system also increases Au(111) crystal phase, the catalytic ability against acetylene is further enhanced considerably. As a result, the MOC devices show increased sensing performance at a reduced optimal operating temperature.

For the Cu<sup>2+</sup>/Au co-doped SnO<sub>2</sub> MOC devices, the monotonous decrease of gas response with increasing the sensor temperature can be explained by the increased Au (111)

phase and electrical resistance of Cu<sup>2+</sup>/Au co-doped SnO<sub>2</sub> nanofibers.

## Conclusions

A simple route to lower the working temperature meanwhile increase the sensitivity of MOCs has been developed based on Cu<sup>2+</sup>/Au co-doped SnO<sub>2</sub> nanofibers. A synergistic effect was found between Cu<sup>2+</sup> and Au, making the co-doped nanofibers have an unexpectedly high gas sensitivity at low optimal working temperature. Co-doping may form a novel strategy to development of ultrasensitive MOCs with low optimal working temperature.

## Notes and references

<sup>a</sup> Institute for Frontier materials, Deakin University, Geelong, Victoria 3216, Australia, Tel: 61 3 52271245; Email: [tong.lin@deakin.edu.au](mailto:tong.lin@deakin.edu.au)

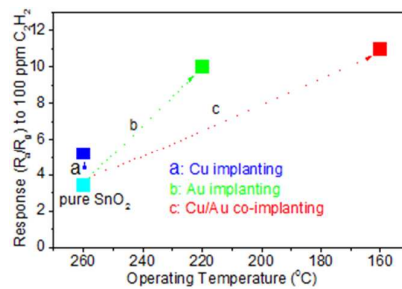
<sup>b</sup> Alan G. MacDiarmid Institute, Jilin University, Changchun 130012, P. R. China.

†Electronic Supplementary Information (ESI) available: details of SEM and TEM images, comparison between different MOCs against C<sub>2</sub>H<sub>2</sub>, XRD patterns, and SnO<sub>2</sub> grain size. See DOI: 10.1039/b000000x/

1. G. Eranna, B. C. Joshi, D. P. Runthala and R. P. Gupta, *Critical Reviews in Solid State and Materials Sciences*, 2004, **29**, 111-188.
2. M. Batzill and U. Diebold, *Progress in Surface Science*, 2005, **79**, 47-154.
3. M. E. Franke, T. J. Koplín and U. Simon, *Small*, 2006, **2**, 36-50.
4. N. Barsan, D. Koziej and U. Weimar, *Sensors and Actuators B-Chemical*, 2007, **121**, 18-35.
5. G. Korotcenkov, *Materials Science and Engineering B-Solid State Materials for Advanced Technology*, 2007, **139**, 1-23.
6. N. Barsan, M. Schweizer-Berberich and W. Göpel, *Fresenius Journal of Analytical Chemistry*, 1999, **365**, 287-304.
7. A. Kolmakov and M. Moskovits, *Annual Review of Materials Research*, 2004, **34**, 151-180.
8. A. Rothschild and Y. Komem, *Journal of Applied Physics*, 2004, **95**, 6374-6380.
9. D. H. Zhang, Z. Q. Liu, C. Li, T. Tang, X. L. Liu, S. Han, B. Lei and C. W. Zhou, *Nano Letters*, 2004, **4**, 1919-1924.
10. A. Kolmakov, D. O. Klenov, Y. Lilach, S. Stemmer and M. Moskovits, *Nano Letters*, 2005, **5**, 667-673.
11. E. Comini, *Analytica Chimica Acta*, 2006, **568**, 28-40.
12. I. D. Kim, A. Rothschild, B. H. Lee, D. Y. Kim, S. M. Jo and H. L. Tuller, *Nano Letters*, 2006, **6**, 2009-2013.
13. M. Paulose, O. K. Varghese, G. K. Mor, C. A. Grimes and K. G. Ong, *Nanotechnology*, 2006, **17**, 398-402.
14. G. Korotcenkov, *Materials Science & Engineering R-Reports*, 2008, **61**, 1-39.
15. K. Yu, Z. Wu, Q. Zhao, B. Li and Y. Xie, *The Journal of Physical Chemistry C*, 2008, **112**, 2244-2247.
16. E. Comini, C. Baratto, G. Faglia, M. Ferroni, A. Vomiero and G. Sberveglieri, *Progress in Materials Science*, 2009, **54**, 1-67.
17. J. H. Lee, *Sensors and Actuators B-Chemical*, 2009, **140**, 319-336.
18. B. Y. Wei, M. C. Hsu, P. G. Su, H. M. Lin, R. J. Wu and H. J. Lai, *Sensors and Actuators B-Chemical*, 2004, **101**, 81-89.

19. C. Bittencourt, A. Felten, E. H. Espinosa, R. Ionescu, E. Llobet, X. Corteig and J. J. Pireaux, *Sensors and Actuators B-Chemical*, 2006, **115**, 33-41.
20. C. Balazsi, K. Sedlackova, E. Llobet and R. Ionescu, *Sensors and Actuators B-Chemical*, 2008, **133**, 151-155.
21. G. H. Lu, L. E. Ocola and J. H. Chen, *Advanced Materials*, 2009, **21**, 2487-+.
22. G. Singh, A. Choudhary, D. Haranath, A. G. Joshi, N. Singh, S. Singh and R. Pasricha, *Carbon*, 2012, **50**, 385-394.
23. S. Deng, V. Tjoa, H. M. Fan, H. R. Tan, D. C. Sayle, M. Olivo, S. Mhaisalkar, J. Wei and C. H. Sow, *Journal of the American Chemical Society*, 2012, **134**, 4905-4917.
24. Q. W. Huang, D. W. Zeng, H. Y. Li and C. S. Xie, *Nanoscale*, 2012, **4**, 5651-5658.
25. P. A. Russo, N. Donato, S. G. Leonardi, S. Baek, D. E. Conte, G. Neri and N. Pinna, *Angewandte Chemie-International Edition*, 2012, **51**, 11053-11057.
26. S. Srivastava, K. Jain, V. N. Singh, S. Singh, N. Vijayan, N. Dilawar, G. Gupta and T. D. Senguttuvan, *Nanotechnology*, 2012, **23**.
27. Y. Wang, X. Jiang and Y. Xia, *Journal of the American Chemical Society*, 2003, **125**, 16176-16177.
28. K. Yong Shin, H. Seung-Chul, K. Kim, H. Yang, C. Sung-Yool, Y. T. Kim, J. T. Park, C. H. Lee, J. Choi, J. Paek and K. Lee, *Applied Physics Letters*, 2005, **86**, 213105-213105-213103.
29. N. Du, H. Zhang, B. D. Chen, X. Y. Ma, Z. H. Liu, J. B. Wu and D. R. Yang, *Advanced Materials*, 2007, **19**, 1641-1645.
30. J. Su, X.-X. Zou, Y.-C. Zou, G.-D. Li, P.-P. Wang and J.-S. Chen, *Inorganic Chemistry*, 2013, **52**, 5924-5930.
31. E. Comini, G. Faglia and G. Sberveglieri, *Sensors and Actuators B-Chemical*, 2001, **78**, 73-77.
32. S. Mishra, C. Ghanshyam, N. Ram, R. P. Bajpai and R. K. Bedi, *Sensors and Actuators B-Chemical*, 2004, **97**, 387-390.
33. S. W. Fan, A. K. Srivastava and V. P. Dravid, *Applied Physics Letters*, 2009, **95**.
34. J. Gong, Y. H. Li, X. S. Chai, Z. S. Hu and Y. L. Deng, *Journal of Physical Chemistry C*, 2010, **114**, 1293-1298.
35. H. Chen, Y. Liu, C. S. Xie, J. Wu, D. W. Zeng and Y. C. Liao, *Ceramics International*, 2012, **38**, 503-509.
36. G. Sakai, N. Matsunaga, K. Shimano and N. Yamazoe, *Sensors and Actuators B: Chemical*, 2001, **80**, 125-131.
37. H. J. Xia, Y. Wang, F. H. Kong, S. R. Wang, B. L. Zhu, X. Z. Guo, J. Zhang, Y. M. Wang and S. H. Wu, *Sensors and Actuators B-Chemical*, 2008, **134**, 133-139.
38. R. K. Joshi, Q. Hu, F. Am, N. Joshi and A. Kumar, *Journal of Physical Chemistry C*, 2009, **113**, 16199-16202.
39. J. Zhang, X. H. Liu, S. H. Wu, M. J. Xu, X. Z. Guo and S. R. Wang, *Journal of Materials Chemistry*, 2010, **20**, 6453-6459.
40. X. H. Liu, J. Zhang, L. W. Wang, T. L. Yang, X. Z. Guo, S. H. Wu and S. R. Wang, *Journal of Materials Chemistry*, 2011, **21**, 349-356.
41. N. S. Ramgir, I. S. Mulla and K. P. Vijayamohanan, *Sensors and Actuators B-Chemical*, 2005, **107**, 708-715.
42. K. Jain, R. P. Pant and S. T. Lakshmikummar, *Sensors and Actuators B: Chemical*, 2006, **113**, 823-829.
43. X. Xu, J. Sun, H. Zhang, Z. Wang, B. Dong, T. Jiang, W. Wang, Z. Li and C. Wang, *Sensors and Actuators B: Chemical*, 2011, **160**, 858-863.
44. P. Feng, X. Y. Xue, Y. G. Liu, Q. Wan and T. H. Wang, *Applied Physics Letters*, 2006, **89**.
45. Y. X. Liang, Y. J. Chen and T. H. Wang, *Applied Physics Letters*, 2004, **85**, 666-668.
46. A. C. Patel, S. X. Li, C. Wang, W. J. Zhang and Y. Wei, *Chem. Mat.*, 2007, **19**, 1231-1238.
47. H.-J. Ahn, H.-C. Choi, K.-W. Park, S.-B. Kim and Y.-E. Sung, *The Journal of Physical Chemistry B*, 2004, **108**, 9815-9820.
48. G. Deroubaix and P. Marcus, *Surface and Interface Analysis*, 1992, **18**, 39-46.
49. R. K. Mishra, A. Kushwahab and P. P. Sahay, *RSC Advances*, 2014, **4**, 3904-3912.
50. D. Kohl, *Sensors and Actuators B: Chemical*, 1990, **1**, 158-165.
51. M. C. Kung, R. J. Davis and H. H. Kung, *The Journal of Physical Chemistry C*, 2007, **111**, 11767-11775.
52. P. Montmeat, J.-C. Marchand, R. Lalauze, J.-P. Viricelle, G. Tournier and C. Pijolat, *Sensors and Actuators B: Chemical*, 2003, **95**, 83-89.
53. R. Ludeke, in *Handbook of Surface Science*, eds. K. Horn and M. Scheffler, North-Holland, 2000, pp. 749-862.
54. E. R. Leite, I. T. Weber, E. Longo and J. A. Varela, *Advanced Materials*, 2000, **12**, 965-968.

## TOC



SnO<sub>2</sub> nanofibers after being co-doped with Cu<sup>2+</sup> and Au show considerably enhanced sensing performances at an unexpectedly-decreased operating temperature, and a synergistic effect occurs when the two dopants are introduced together.